Supporting Information

Selective Electrochemical Production of Formate from Carbon Dioxide with Bismuth-Based Catalysts in an Aqueous Electrolyte

Chan Woo Lee,[†,§] *Jung Sug Hong,*[†] *Ki Dong Yang,*[†] *Kyoungsuk Jin,*[†] *Jun Ho Lee,*[†] *Hyo-Yong Ahn,*[†] *Hongmin Seo,*[†] *Nark-Eon Sung,*[‡] *and Ki Tae Nam**[,†]

[†]*Department of Materials Science and Engineering, Seoul National University, Seoul 151-744, Korea*

[‡]*Pohang Accelerator Laboratory, Pohang University of Science and Technology, Pohang, 37673, Republic of Korea*

[§]*Clean Energy Research Center, Korea Institute of Science and Technology (KIST), 5 Hwarang-ro 14-gil, Seongbuk-gu, Seoul 02792, Republic of Korea*

*Correspondence to: nkitae@snu.ac.kr

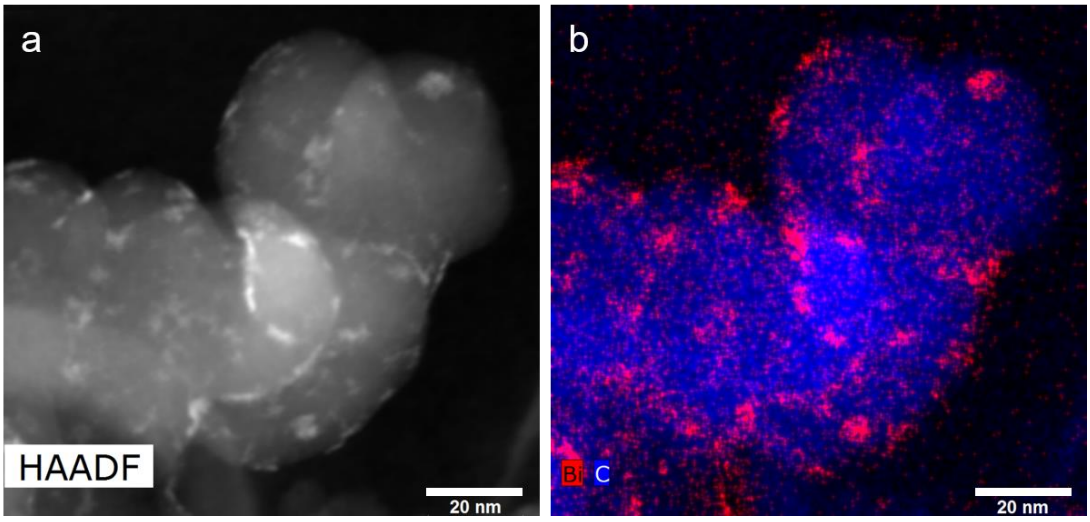

Figure S1. (a) STEM image and (b) EDS elemental mapping of the synthesized BiO_x/C.

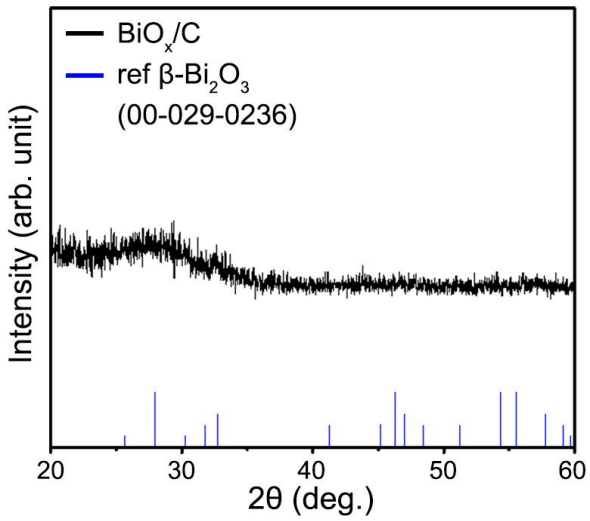

Figure S2. The XRD patterns of the synthesized BiO_x/C.

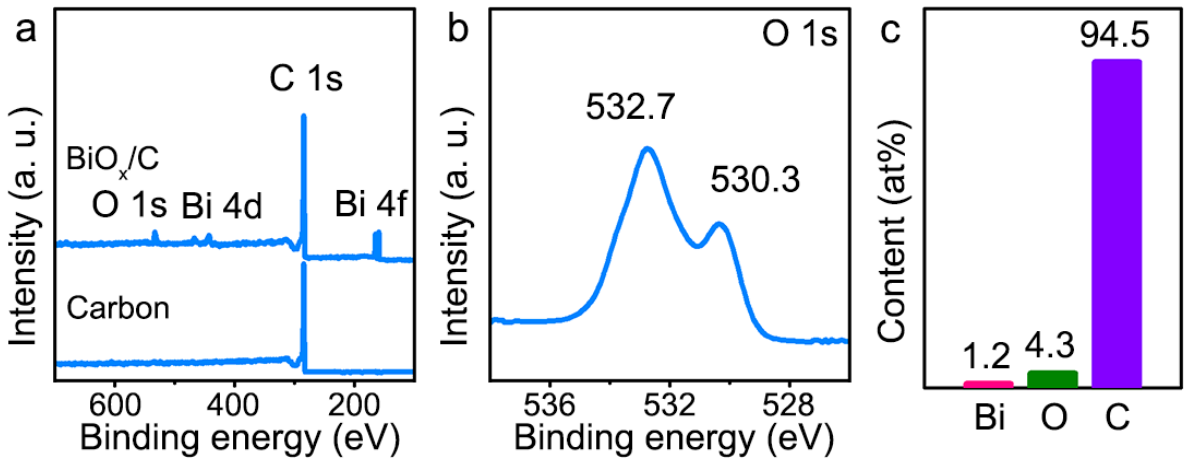

Figure S3. (a) Survey XPS and (b) O 1s spectra of the BiO_x/C. (c) Atomic percentages of Bi, O, and C measured by XPS.

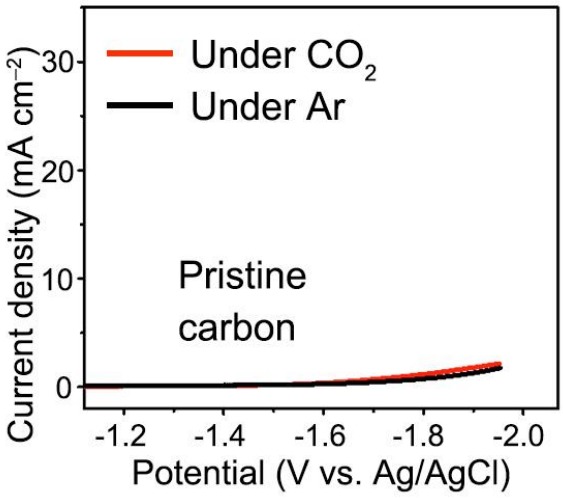

Figure S4. Cathodic linear sweep voltammetric scans of carbon black on glassy carbon plate electrode at 50 mV s^{-1} in 0.5 M $NaHCO_3$/0.5 M $NaClO_4$ under CO_2 and Ar.

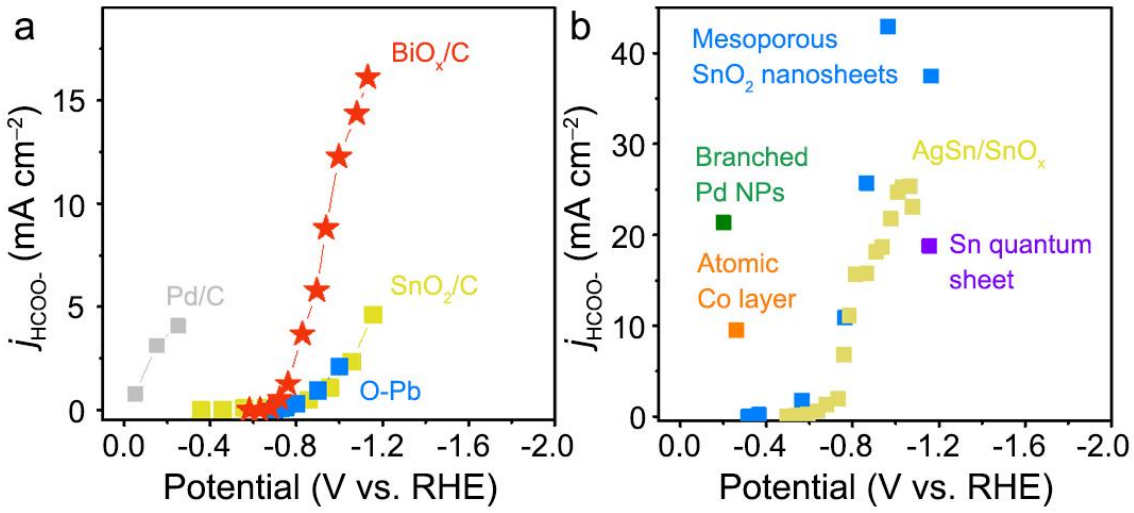

Figure S5. Comparison with reported $HCOO^-$ catalysts. Data of the reported catalysts were extracted or collected from the previous literatures. The Figure S5(a) includes Pd/C, SnO_2/C and PbO_2 particle film for the comparison. The Figure S5(b) includes the current state of the art catalysts for $HCOO^-$ production.

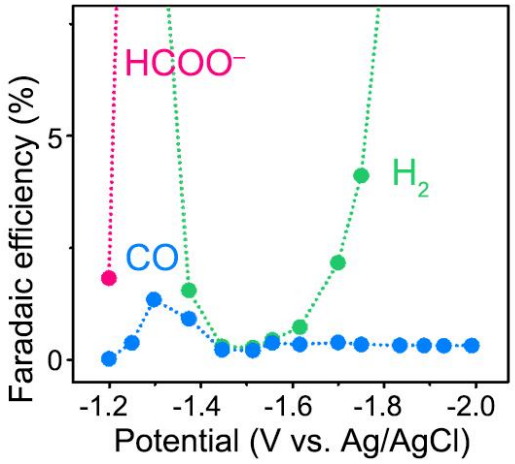

Figure S6. An enlarged view of potential dependence of faradaic efficiencies for $HCOO^-$, H_2 and CO production.

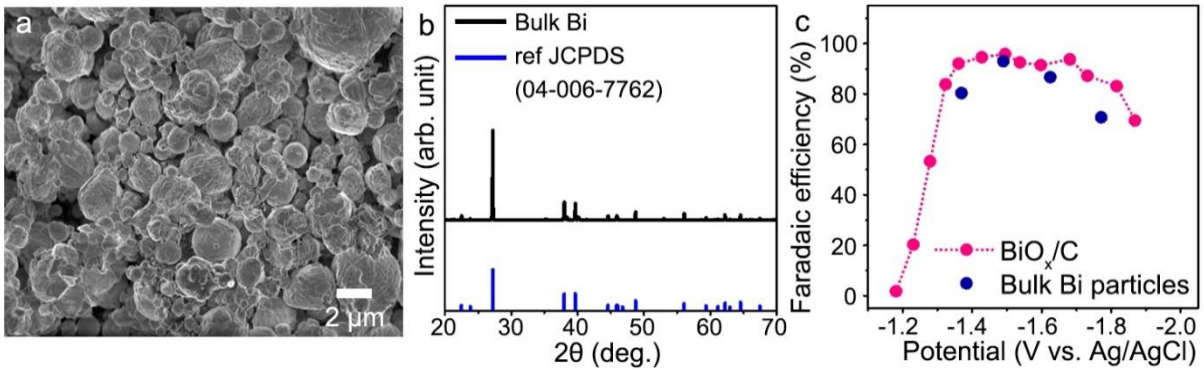

Figure S7. (a) Typical FESEM images and (b) XRD patterns of bulk Bi particles. (c) The faradaic efficiency of bulk Bi particles for $HCOO^-$ at various potentials.

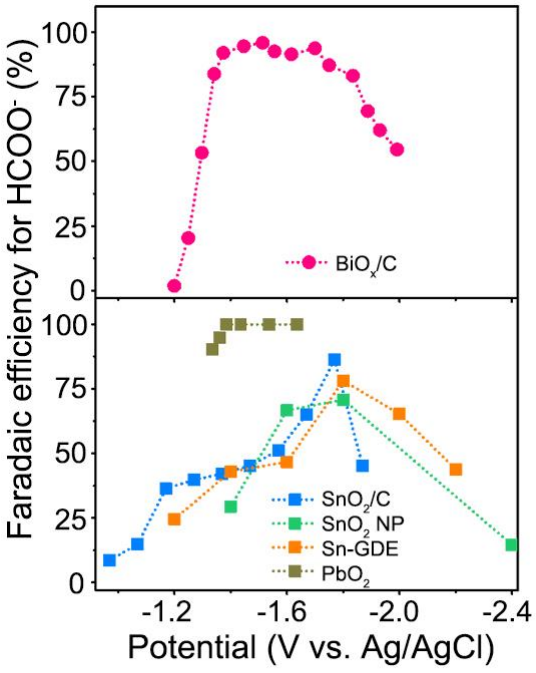

Figure S8. Potential dependence of faradaic efficiency for $HCOO^-$ and comparison with SnO_2/C, SnO_2 NP, Sn-GDE and PbO_2. Data were extracted or collected from the previous literatures.

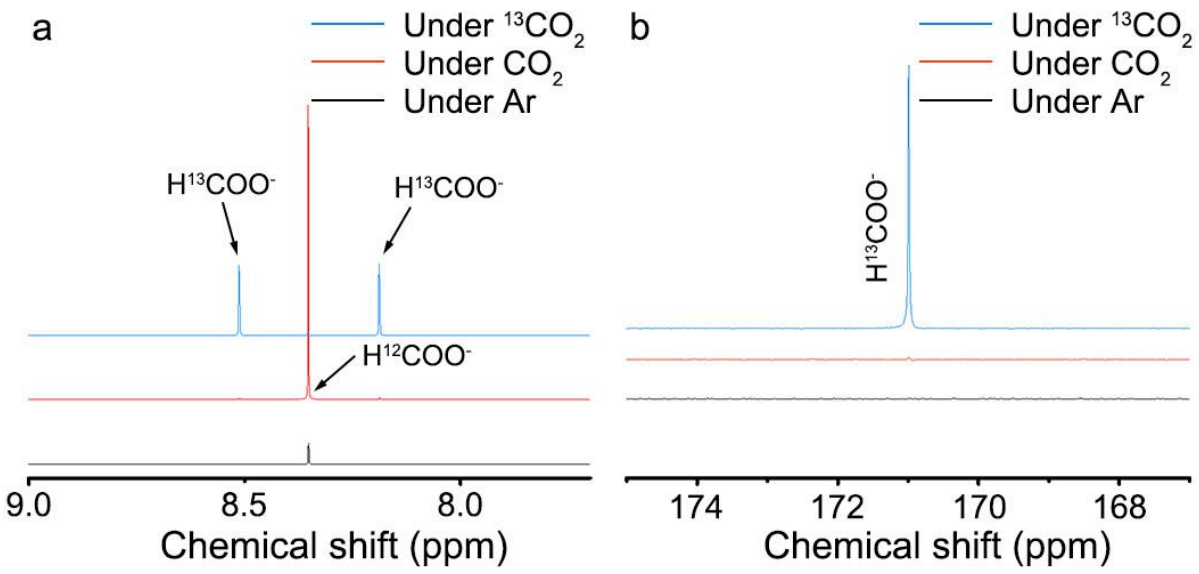

Figure S9. (a) ^{1}H NMR and (b) ^{13}C NMR spectra of the resultant solutions after bulk electrolysis at −1.51 V vs. Ag/AgCl under CO_2, Ar and $^{13}CO_2$ flow.

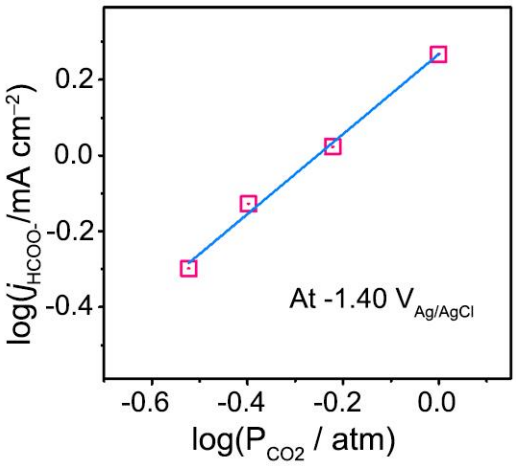

Figure S10. Plot of the partial current density for $HCOO^-$ as a function of the CO_2 partial pressure at the fixed potential. The CO_2 partial pressure was controlled by changing the ratio of the CO_2 and Ar flows (20 cc min^{-1} in total).

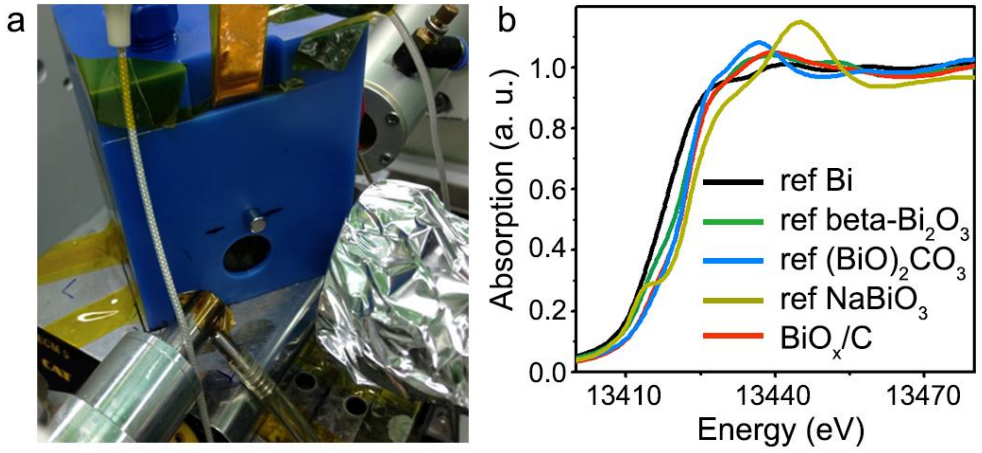

Figure S11. (a) A picture of in situ XANES cell. (b) Normalized Bi L_3-edge XANES spectra of reference Bi, β-Bi_2O_3, $Bi_2O_2CO_3$, $NaBiO_3$ and BiO_x/C.

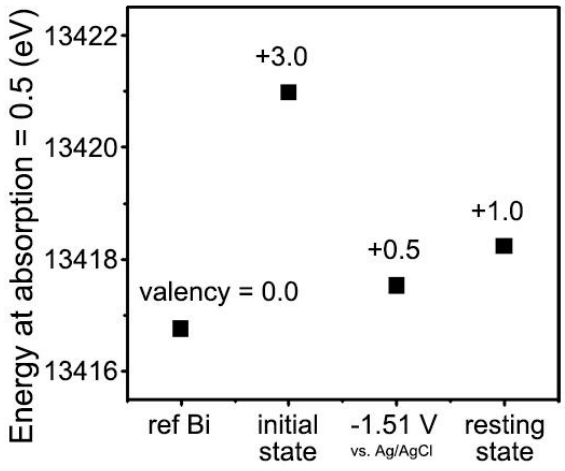

Figure S12. Average Bi valencies of Bi metal and BiO_x/C at the initial state, −1.51 V vs. Ag/AgCl and resting state.

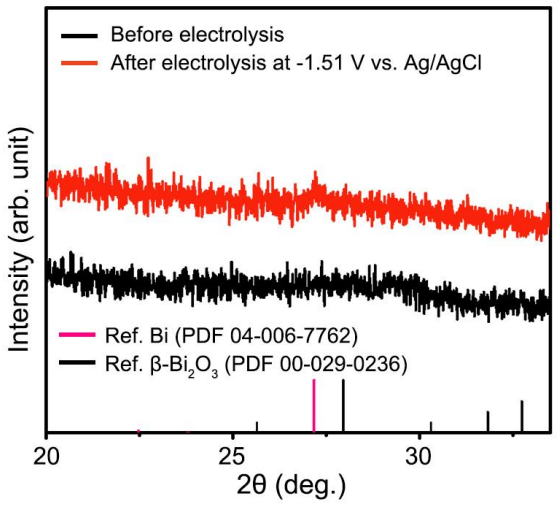

Figure S13. XRD patterns of BiO_x/C before and after electrolysis at −1.51 V vs. Ag/AgCl. Bar graphs at the bottom represent the referenced XRD patterns of Bi metal (pink) and β-Bi_2O_3 (black).

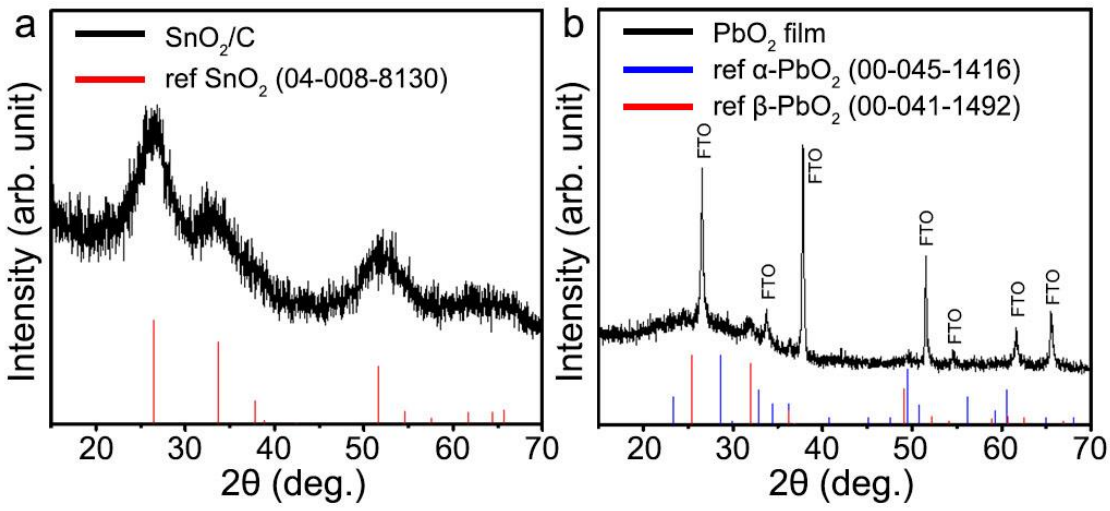

Figure S14. XRD patterns of (a) SnO_2/C powder and (b) PbO_2 film which were synthesized using the experimental methods reported from previous literatures. For XRD analysis, the PbO_2 film was electrodeposited on FTO glass. Bar graphs at the bottom represent the referenced XRD patterns of SnO_2, α-PbO_2 and β-PbO_2.

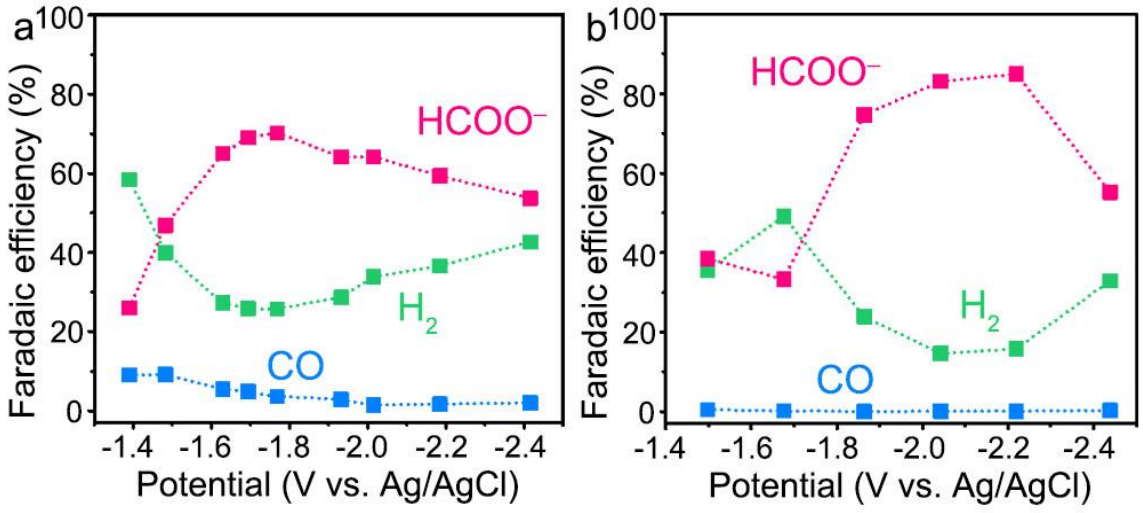

Figure S15. Potential dependence of Faradaic efficiencies for $HCOO^-$, H_2, and CO production in CO_2-saturated 0.1 M $NaHCO_3$/0.9 M $NaClO_4$ on (a) SnO_2/C and (b) PbO_2 film electrodes. The SnO_2/C was dispersed in ethanol with Nafion and drop-coated on a glassy carbon plate. The PbO_2 film was directly electrodeposited on a glassy carbon plate electrode.

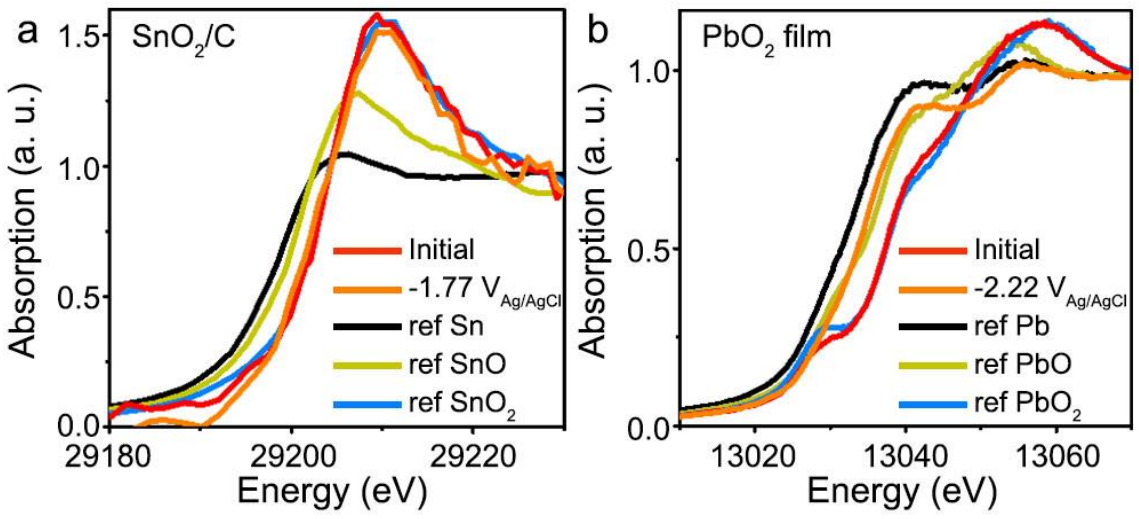

Figure S16. (a) Normalized Sn K-edge XANES spectra of ref Sn, ref SnO, ref SnO_2, and SnO_2/C at the initial state and –1.77 V vs. Ag/AgCl. (b) Normalized Pb L3-edge XANES spectra of ref Pb, ref PbO, ref PbO_2, and PbO_2 film at the initial state and –2.22 V vs. Ag/AgCl. The electrolysis was conducted at the potentials achieving a maximum faradaic efficiency for $HCOO^-$.

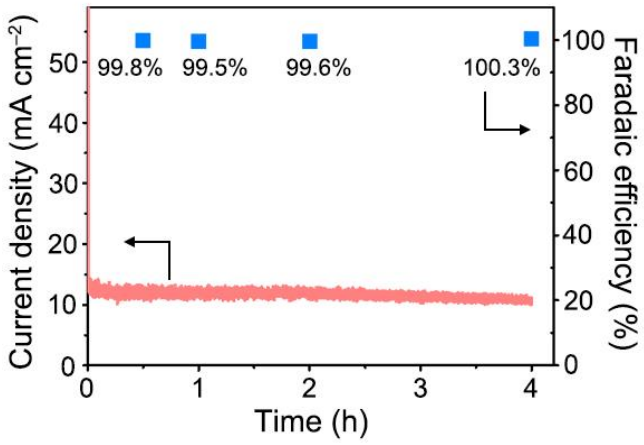

Figure S17. Total current densities and Faradaic efficiencies for $HCOO^-$ as a function of time at −1.65 V vs. Ag/AgCl in 0.5 M NaCl.

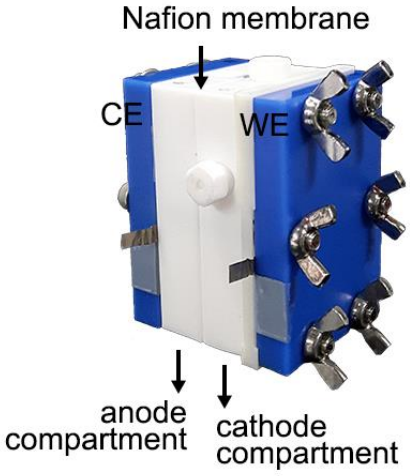

Figure S18. A picture of CO_2 reduction cell used in this study. The cell consists of cathode and anode compartments with a piece of Nafion membrane. The working and counter electrodes are inserted between white and blue plates. The separator is inserted between two compartments.